# Supporting Information

## Unveiling the Photophysical Mechanisms in Low-Dimensional Zn/Cu-Based Metal Halides

*Chuanyao Yang,[a] Jia Zheng,[a,c] Chang Xu,[a,d] Chong, Xiao,[a] Yuanyuan Chang,[e] Lei Zhou*[b], Xiangnan Gong*[a]*

[a] Analytical and Testing Center of Chongqing University, Chongqing, 401331, P.R. China

[b] Chongqing Key Laboratory of Soft-Matter Materials Manufacturing, School of Chemistry and Chemical Engineering, Southwest University, Chongqing, 400715, P.R. China

[c] College of Environment and Ecology, Chongqing University, Chongqing 400045, P.R. China

[d] College of Physics, Chongqing University, Chongqing, 401331, P.R. China

[e] Institute of Materials Science and Devices, School of Materials Science and Engineering, Suzhou University of Science and Technology, Suzhou, 215009 P. R. China

*** Corresponding authors:** Lei Zhou, E-mail: zhoulei25@swu.edu.cn

Xiangnan Gong, E-mail: xiangnan.gong@cqu.edu.cn

## EXPERIMENTAL SECTION

**Materials.** Zinc bromide ($ZnBr_2$, 99.99%, Alfa Aesar), Cupric bromide ($CuBr_2$, 99%, Sigma-Aldrich), 2,3-Dimethylpyrazine ($C_6H_8N_2$, 98%, Aladdin), 2,3,5-Trimethylpyrazine ($C_7H_{10}N_2$, 99%, Aladdin), Other organics are analytical reagents.

**Crystals Growth.** $(C_6H_8N_2)_2ZnBr_2$ crystals were prepared by a solvent evaporation method (Fig. S1a). First, 0.1 mmol of $ZnBr_2$ was dissolved in 10 mL ethanol in a crystallization cell, followed by sonication for 5 minutes to ensure complete dissolution. Subsequently, 1 mL of 2, 3-Dimethylpyrazine or an alternative such as 2-ethylpyrazine and 2, 3, 5-Trimethylpyrazine was added, followed by additional ultrasonic treatment and 24 hours of stirring. The jar was then sealed and small holes were pierced to allow it to slowly evaporate under cool, shaded conditions over approximately 10 days to facilitate crystal growth.

$(C_7H_{10}N_2)CuBr_2$ crystals were prepared using the gaseous diffusion method (Fig. S1b). Initially, 0.1 mmol $CuBr_2$ was dissolved and sonicated in 10 mL acetone in a tube, which was then placed into a sealed container containing dichloromethane. 1 mL of 2, 3, 5-Trimethylpyrazine was added in dichloromethane and mixed evenly. As the dichloromethane slowly evaporated over approximately 10 days, the solubility of the substances in the tube decreased and crystals precipitated. Crystals were successfully prepared after the solvent was poured out from the tube and evaporated.

**Characterization.** Single crystal X-ray diffraction was recorded with a SuperNova (Agilent Technologies Inc., USA). Powder X-ray diffraction (PXRD) was carried out on a PANalytical X' Pert Powder with a Cu Kα X-ray (λ=1.54056 Å) tube operated at 40 mA, 40 kV and with

scan steps and diffraction ranges of 0.026 and 5° to 60°, respectively. Attenuated total reflection (ATR) infrared spectra in the region 4000 to 400 $cm^{-1}$ were recorded using a Nicolet iS50 instrument (Thermo Fisher Scientific, USA). The corresponding compositions of the samples were examined by a tungsten filament scanning electron microscope TM4000Plus II (Hitachi, Ltd., JP) equipped with an attached energy dispersive spectrometer (EDS). XPS measurements of the samples were conducted on a Thermo K-Alpha spectrometer equipped with a monochromatic Al Kα X-ray source. The UV-Vis absorption spectra of the prepared samples were characterized using a Shimadzu UV3700 UV-Vis spectrophotometer. The excitation and emission spectra and the decay curves were measured with an FLS1000 fluorescence spectrometer. (Edinburgh Instruments Ltd., U.K). The thermogravimetric and differential scanning calorimeter (TG-DSC) data was implemented on a TGA2 (Mettler Toledo, Switzerland).

PLQYs were measured with an FLS1000 fluorescence spectrometer with an integrating sphere attachment. To begin, a PL spectrum of a blank (without a sample) was tested using the integrating sphere. Next, a PL spectrum of the sample was tested using the integrating sphere. Finally, the PLQY was calculated using the following formula:

$$PLQY = \frac{E_S - E_B}{S_B - S_S} \quad (1)$$

Where the $E_B$ and $E_S$ are photon counts corresponding to emission spectra of the sphere background and sample separately. The $S_B$ and $S_S$ are photon counts corresponding to excitation Rayleigh scattering spectra of sphere background and sample separately.

In addition, the PL decay curves were fitted by a double exponential, and the fitting formula is as follows:

$$A(t) = A_1 e^{-\frac{t}{\tau 1}} + A_2 e^{-\frac{t}{\tau 2}} \quad (2)$$

$$\tau_{average} = \frac{A_1 {\tau_1}^2 + A_2 {\tau_2}^2}{A_1 \tau_1 + A_2 \tau_2} \quad (3)$$

where $A_1$ and $A_2$ are the amplitudes (or weighing factors), and $\tau_1$ and $\tau_2$ are the corresponding lifetimes.

To quantitatively understand the thermal behavior of excitons within these materials, the exciton binding energy ($E_b$) was calculated using the Arrhenius equation.[1, 2]

$$I(T) = \frac{I_0}{1 + Aexp\left(-\frac{E_b}{k_B T}\right)} \#(1)$$

Where $I_0$ is the PL intensity at 0 K, $E_b$ is the exciton binding energy, and $K_b$ is the Boltzmann constant. $E_b$ values represent the need energy for the exciton transition from the bound state to the free state.

Huang-Rhys factor ($S$) is obtained to evaluate the intensity of electron-phonon coupling, according to the following equation:

$$FWHM = 2.36\sqrt{S}\hbar\omega_{phonon}\sqrt{\frac{\coth\left(\hbar\omega_{phonon}\right)}{2k_B T}} \#(2)$$

Where $\hbar$ is Planck's constant, $\omega_{phonon}$ represents the phonon frequency.

**Table S1.** Single crystal X-ray diffraction data of $(C_6H_8N_2)_2ZnBr_2$.

| Compound | $(C_6H_8N_2)_2ZnBr_2$ | $(C_7H_{10}N_2)CuBr_2$ |
|---|---|---|
| Formula weight | 220.74 | 172.76 |
| Temperature/K | 200.00 (10) | 293 (2) |
| Crystal system | monoclinic | monoclinic |
| Space group | C2/c | $P2_1/m$ |
| a/Å | 7.0944 (3) | 6.7527 (5) |
| b/Å | 12.2277 (4) | 8.6037 (9) |
| c/Å | 18.1167 (7) | 9.2040 (8) |
| α/° | 90 | 90 |
| β/° | 92.812 (4) | 98.410 (9) |
| γ/° | 90 | 90 |
| Volume/Å$^3$ | 1569.70 (10) | 528.99 (8) |
| Z | 8 | 4 |
| $\rho_{calc}$g/cm$^3$ | 1.868 | 2.169 |
| μ/mm$^{-1}$ | 6.647 | 9.568 |
| F(000) | 864.0 | 330.0 |
| Crystal size/mm$^3$ | 0.35 × 0.34 × 0.3 | 0.28 × 0.05 × 0.04 |
| Radiation | Mo Kα (λ = 0.71073) | Mo Kα (λ = 0.71073) |
| 2Θ range for data collection/° | 6.664 to 57.918 | 7.018 to 52.702 |
| Index ranges | -8 ≤ h ≤ 9, -16 ≤ k ≤ 16, -24 ≤ l ≤ 23 | -8 ≤ h ≤ 8, -10 ≤ k ≤ 9, -11 ≤ 11 |
| Reflections collected | 5890 | 2108 |
| Independent reflections | 1869 [$R_{int}$= 0.0583, $R_{sigma}$= 0.0669] | 1157 [$R_{int}$= 0.0196, $R_{sigma}$= 0.0357] |
| Data/restraints/parameters | 1869/0/89 | 1157/0/73 |
| Goodness-of-fit on $F^2$ | 1.031 | 1.041 |
| Final R indexes [I>=2σ (I)] | $R_1$= 0.0506, $wR_2$= 0.1209 | $R_1$= 0.0537, $wR_2$= 0.1342 |
| Final R indexes [all data] | $R_1$= 0.0688, $wR_2$= 0.1367 | $R_1$= 0.0740, $wR_2$= 0.1510 |
| Largest diff. peak/hole / e Å$^{-3}$ | 1.05/-1.23 | 2.83/-0.58 |

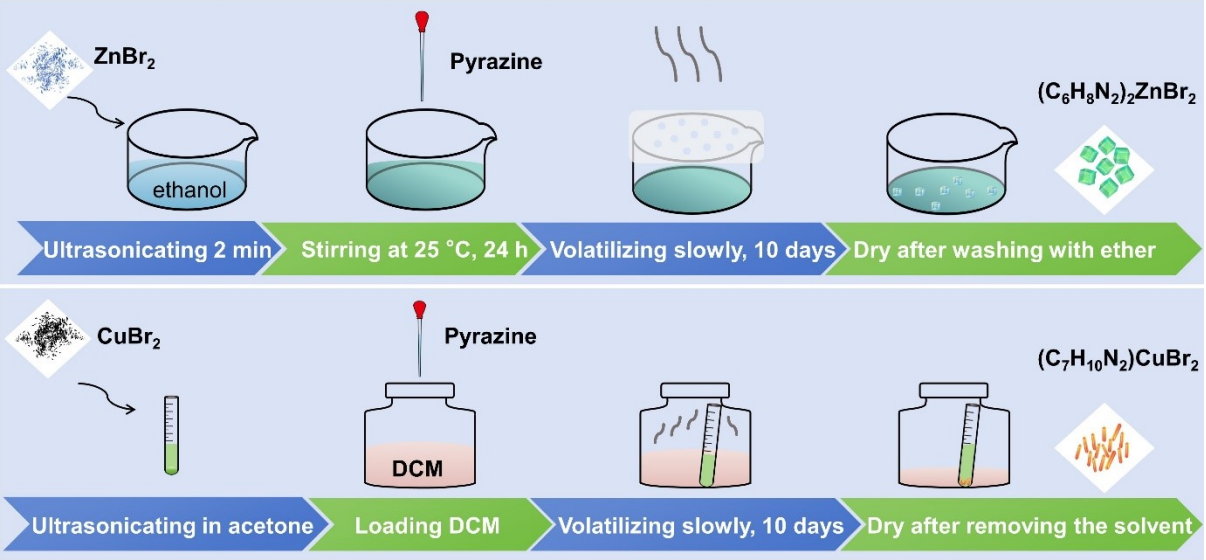


**Fig. S1** (a) Schematic of solvent evaporation method to synthesize $(C_6H_8N_2)_2ZnBr_2$ crystals. (b) Schematic of gaseous diffusion method to synthesize $(C_7H_{10}N_2)CuBr_2$ crystals.

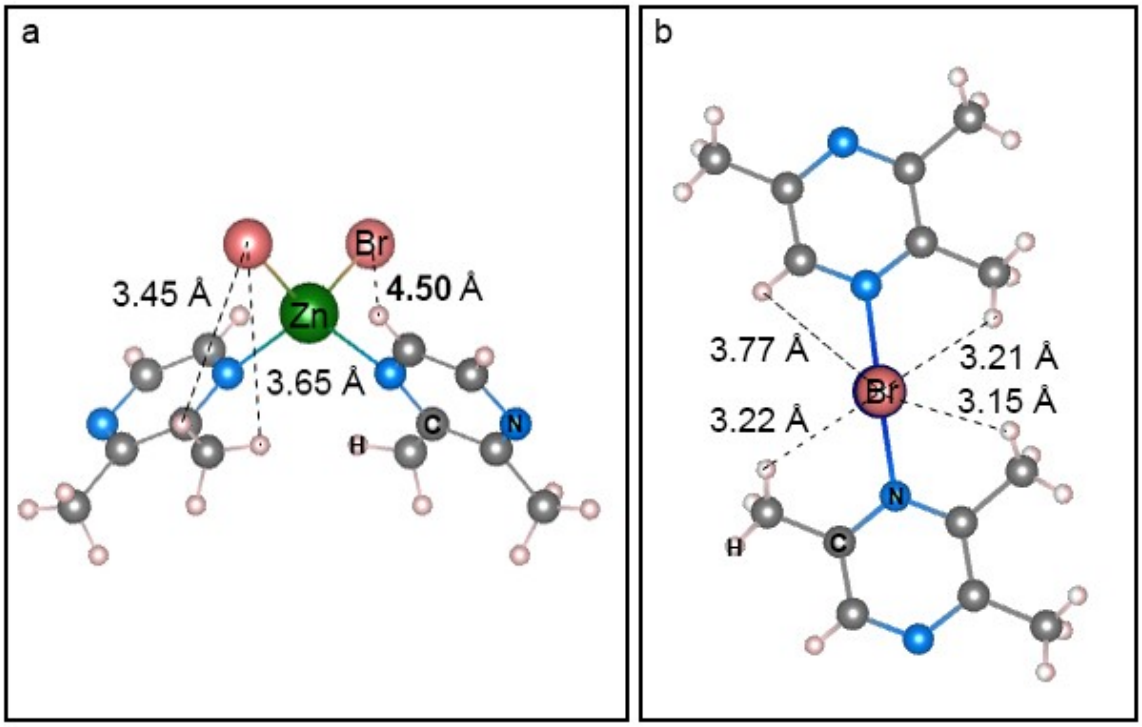


**Fig. S2** Regarding the bond lengths of H-Br bonds at different spatial positions in (a) $(C_6H_8N_2)_2ZnBr_2$ and (b) $(C_7H_{10}N_2)CuBr_2$.

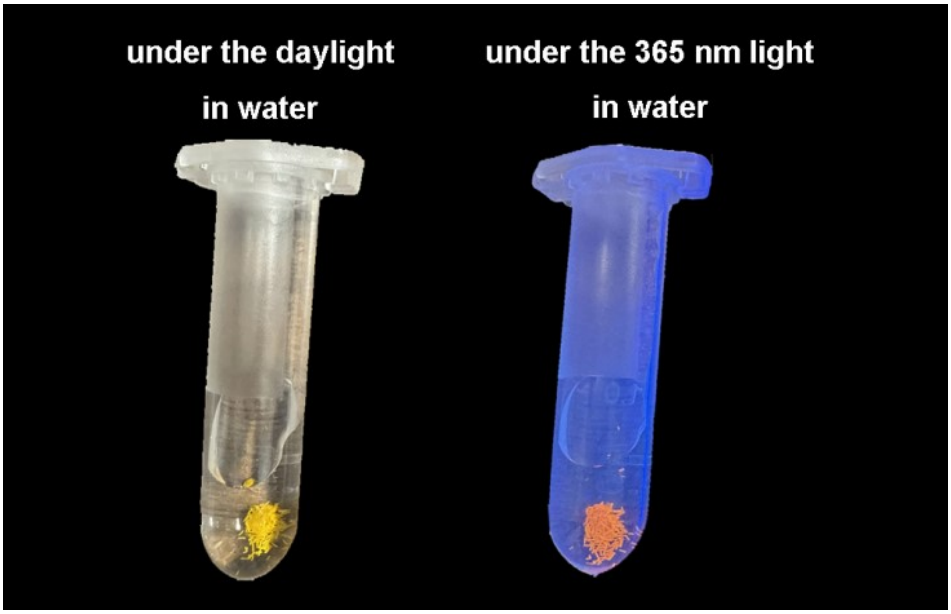


**Fig. S3** Photographs of $(C_7H_{10}N_2)CuBr_2$ crystals in water over 60 days.

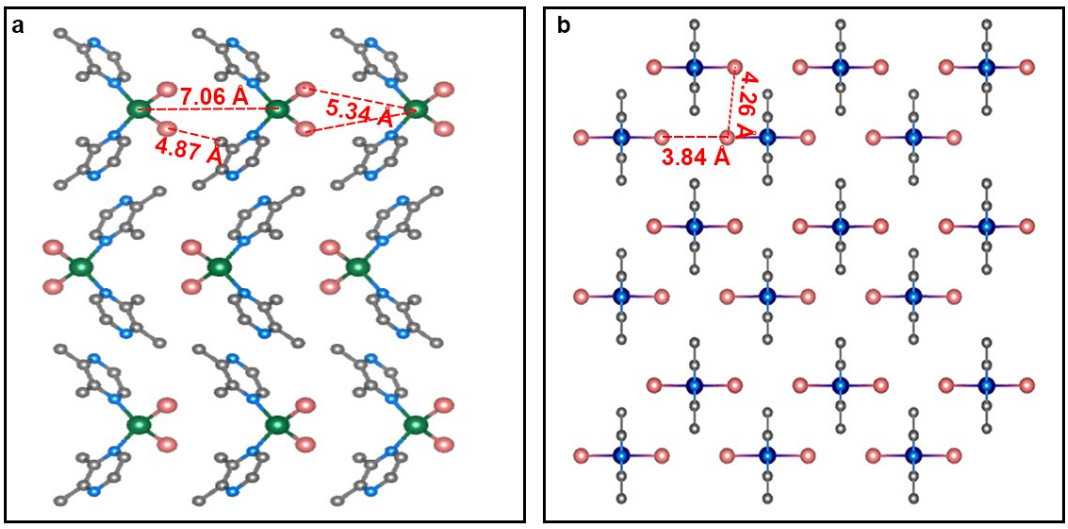


**Fig. S4** The measured intermolecular interstice of (a) $(C_6H_8N_2)_2ZnBr_2$ and (b) $(C_7H_{10}N_2)CuBr_2$. The results indicate that $(C_6H_8N_2)_2ZnBr_2$ exhibits much larger intermolecular interstice that might result in its structure dissolution in water.

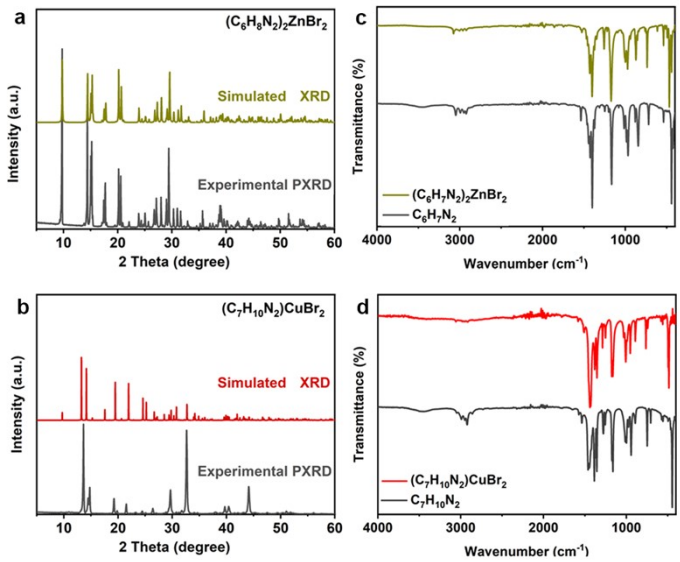


**Fig. S5** (a) Simulated SCXRD and experimental PXRD patterns of $(C_6H_8N_2)_2ZnBr_2$ crystals. (b) Simulated SCXRD and experimental PXRD patterns of $(C_7H_{10}N_2)CuBr_2$ crystals. (c) ATR infrared spectra of $(C_6H_8N_2)_2ZnBr_2$ and the organic salt. (d) ATR infrared spectra of $(C_7H_{10}N_2)CuBr_2$ and the organic salt.

The powder X-ray diffractions of the two compounds align with the simulated results derived from single crystal data, confirming their high phase purity (Fig. S5 a, b). The infrared spectra exhibit distinct transmittance peaks corresponding to the organic cations (Fig. S5 c, d), which underscores the presence and stability of the organic components within the crystalline framework.

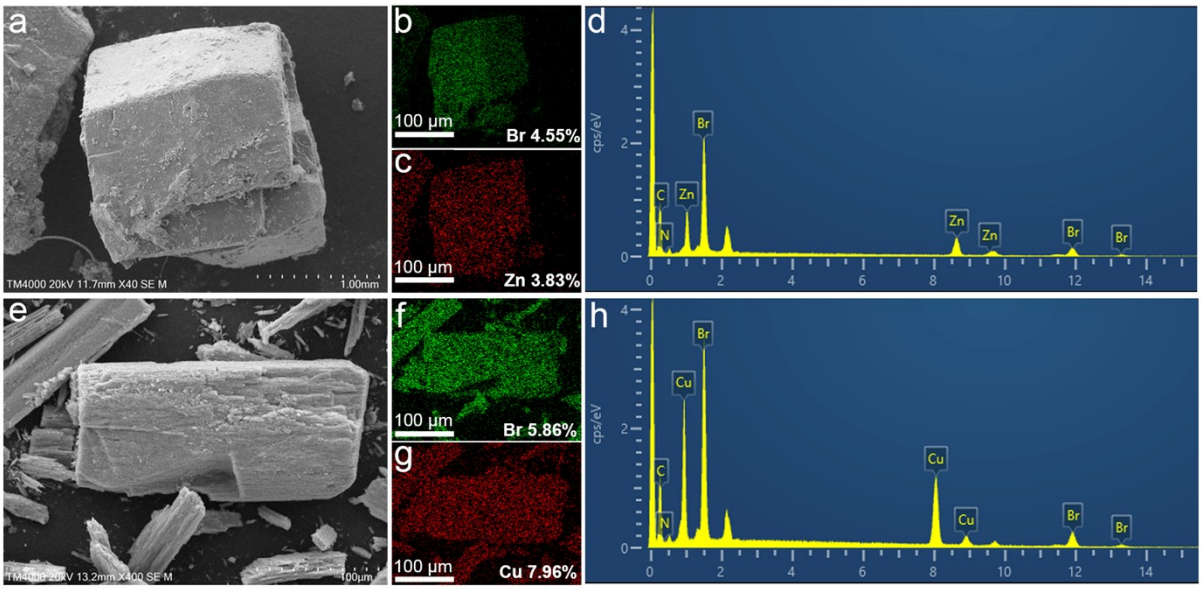


**Fig. S6** (a) SEM images of $(C_6H_8N_2)_2ZnBr_2$ crystals. (b) the distribution of Br element in $(C_6H_8N_2)_2ZnBr_2$. (c) the distribution of Zn element in $(C_6H_8N_2)_2ZnBr_2$. (d) The EDS of $(C_6H_8N_2)_2ZnBr_2$. (e) SEM images of (C7H10N2)CuBr2 crystals. (f) the distribution of Br element in $(C_7H_{10}N_2)CuBr_2$. (g) the distribution of Zn element in $(C_7H_{10}N_2)CuBr_2$. (h) The EDS of $(C_7H_{10}N_2)CuBr_2$.

As shown in the SEM images, $(C_6H_8N_2)_2ZnBr_2$ crystals crystallize in block shapes, whereas form a needle-like shape. EDS unveils the homogeneous elemental distributions throughout the bulk material (Fig. S5). The approximation ratio of Br/Zn is 1/1, while the Br/Cu is 0.8:1. The slight deficiency in Br for $(C_7H_{10}N_2)CuBr_2$ crystals could be attributed to the release of halogens during the crystallization process.

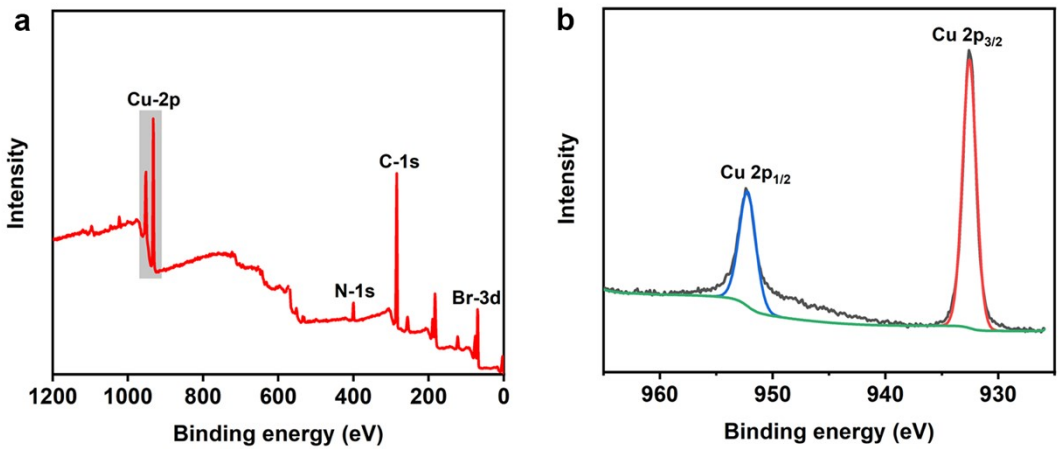


**Fig. S7** (a) XPS spectrum for the $(C_7H_{10}N_2)CuBr_2$ crystals. (b) Cu 2p XPS spectrum.

X-ray photoelectron spectroscopy (XPS) was measured to determine the valence state of copper ions. The measured high-resolution Cu spectrum consists of a pair separated by the Cu 2p spin-orbit splitting (Fig. S6), each of which has a well-resolved single component at 932.5 and 952.3 eV, respectively, confirming the +1 oxidation state of Cu.[3-6]

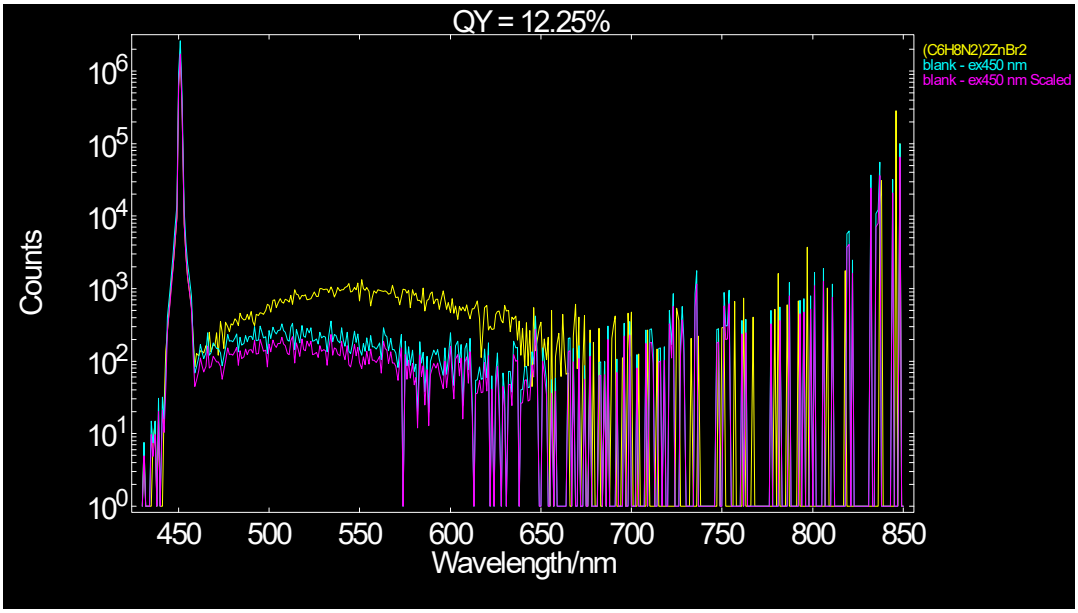


**Fig. S8** The PLQY of $(C_6H_8N_2)_2ZnBr_2$.

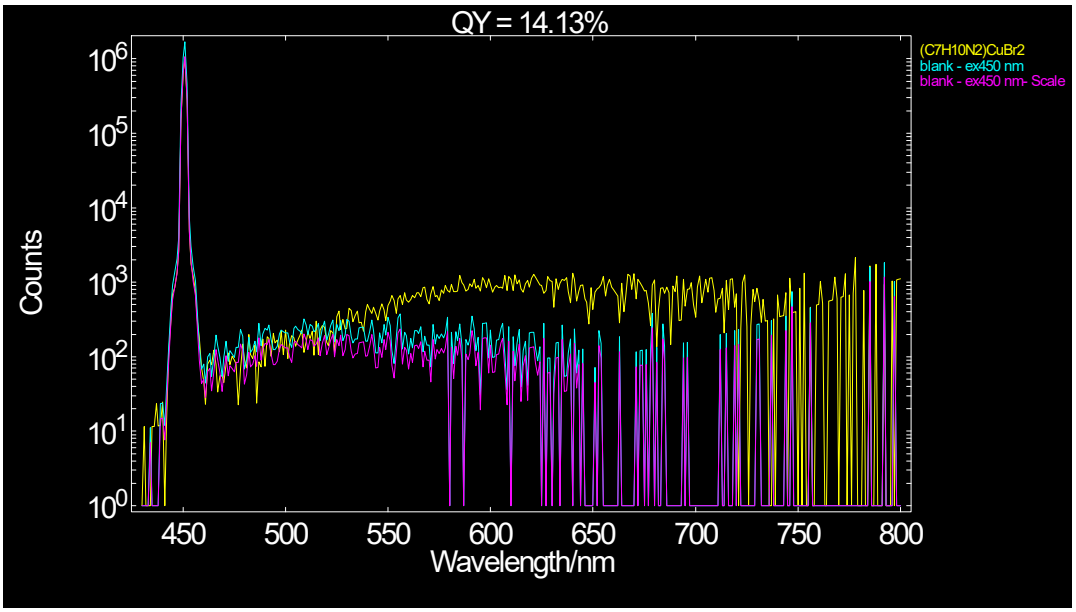


**Fig. S9** The PLQY of $(C_7H_{10}N_2)CuBr_2$.

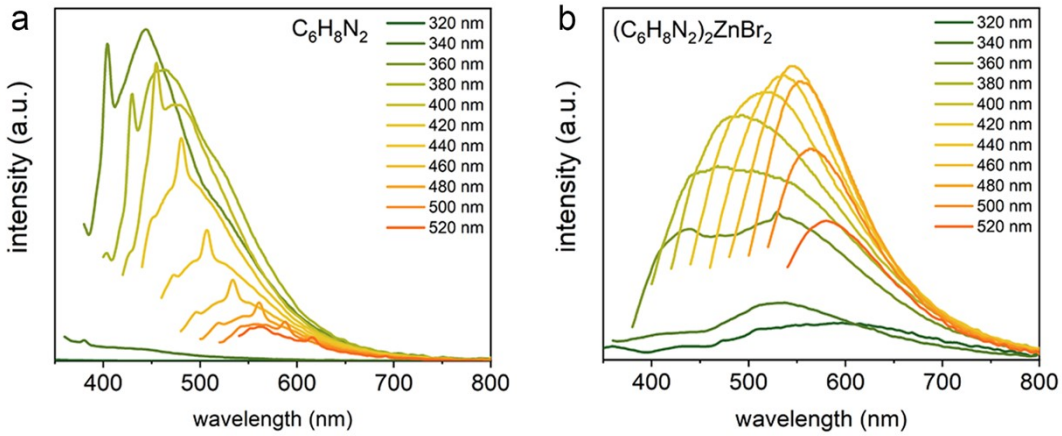


**Fig. S10** (a) The emission spectra of $C_6H_8N_2$ and (b) $(C_6H_8N_2)_2ZnBr_2$ in different excitation wavelengths.

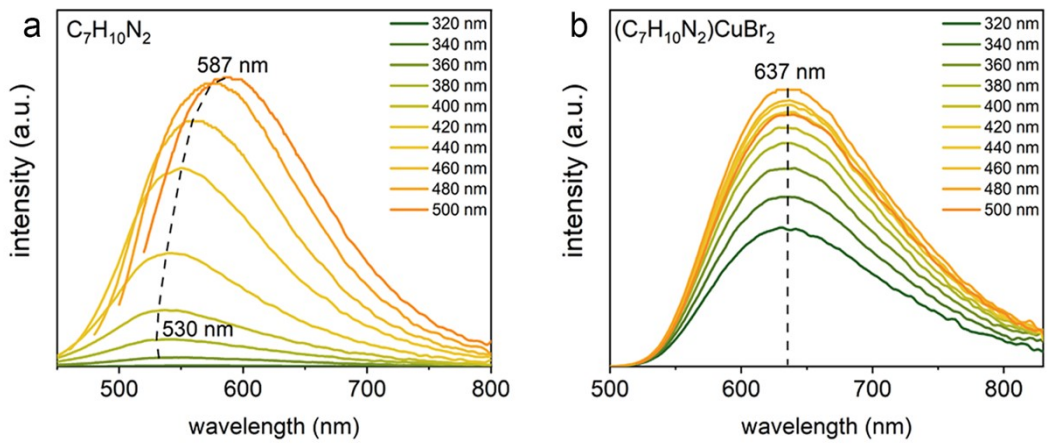


**Fig. S11** (a) The emission spectra of $C_7H_{10}N_2$ and (b) $(C_7H_{10}N_2)CuBr_2$ in different excitation wavelengths.

The PL properties of $(C_7H_{10}N_2)CuBr_2$ are distinctively different from that of the corresponding organic cation ($C_7H_{10}N_2$), ruling out the emission from $C_7H_{10}N_2$, and providing a hint that $Cu^+$ ions may be the emission center. Unlike the multiple emissions in Cu(I)-based organometallic halides that usually originate from the metal center (MC), metal-to-ligand charge transfer (MLCT), and ligand-to-metal charge transfer (LMCT),[7, 8] $(C_7H_{10}N_2)CuBr_2$ exhibits only a single emission at different excitation wavelength and temperatures. Similar to the majority of Cu(I)-based luminescent materials, the emission in $(C_7H_{10}N_2)CuBr_2$ might be originated from STEs. The STEs are likely stabilized by the unique crystal structure and strong electron-phonon coupling, which results in a broad emission band and long photoluminescence lifetimes.[9, 10]

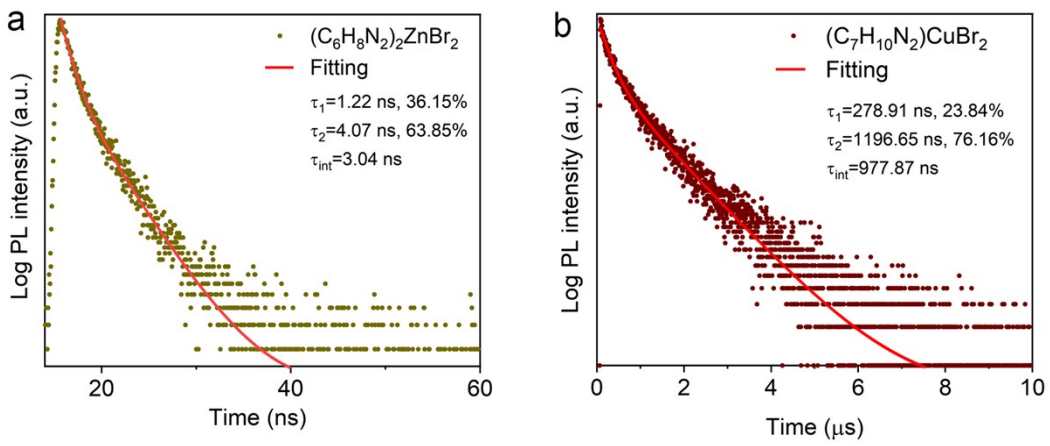


**Fig. S12** (a) Time-resolved photoluminescence (TRPL) decay curves of the $(C_6H_8N_2)_2ZnBr_2$ and (b) the $(C_7H_{10}N_2)CuBr_2$.

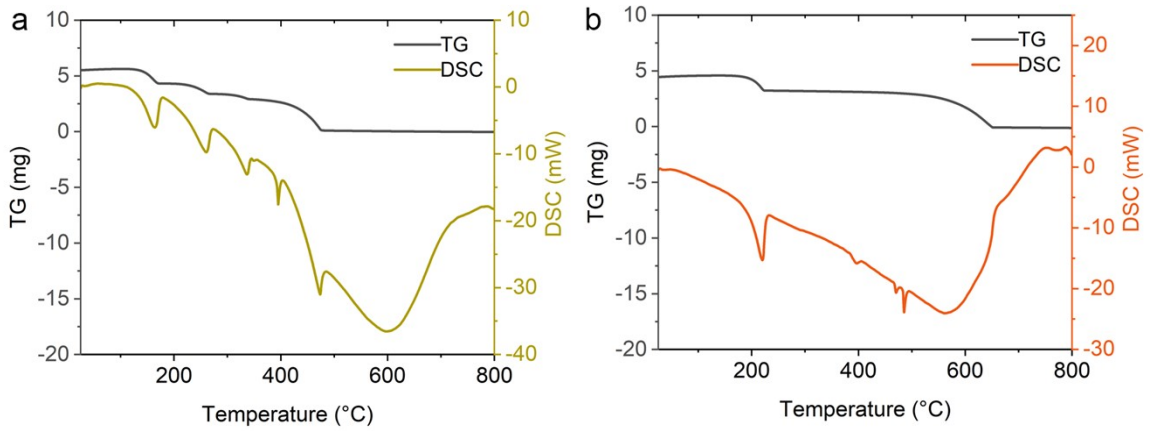


**Fig. S13** TGA-DSC data of (a) $(C_6H_8N_2)_2ZnBr_2$ and (b) $(C_7H_{10}N_2)CuBr_2$ crystals from 25 to 800 °C with a heating rate of 10 °C $min^{-1}$.

# reference


1. H. Wu, R. Zeng, Z. Tang, Y. Bai, S. Zhang and Y. Dai, *J. Lumin.*, 2024, **267**, 120403.
2. L. Zhou, M. Ren, R. He and M. Li, *Inorg. Chem.*, 2022, **61**, 5283-5291.
3. X. Meng, S. Ji, Q. Wang, X. Wang, T. Bai, R. Zhang, B. Yang, Y. Li, Z. Shao, J. Jiang, K. Han and F. Liu, *Adv. Sci.*, 2022, **9**, 2203596.
4. J. Hou, J. Wu, Z. Qin, Y. Fang, L. Shen, X. Qiao, L. Dong, G. Zhang, Y. Liu, G. Zhao and H. Chen, *J. Mater. Chem. C*, 2023, **11**, 2137-2143.
5. S. Zhou, Y. Chen, K. Li, X. Liu, T. Zhang, W. Shen, M. Li, L. Zhou and R. He, *Chem. Sci.*, 2023, **14**, 5415-5424.
6. P. Zhang, Z. Yan, C. Li, Y. Du, L. Ma, Z. Wang, T. Lin, L. Zhao and J. Xiao, *Chem. Eng. J.*, 2024, **496**, 154106.
7. J. Huang, B. Su, E. Song, M. S. Molokeev and Z. Xia, *Chem. Mater.*, 2021, **33**, 4382-4389.
8. J. Huang, Y. Peng, J. Jin, M. S. Molokeev, X. Yang and Z. Xia, *J. Phys. Chem. Lett.*, 2021, **12**, 12345-12351.
9. X. Meng, S. Ji, Q. Wang, X. Wang, T. Bai, R. Zhang, B. Yang, Y. Li, Z. Shao, J. Jiang, K. Han and F. Liu, *Adv. Sci.*, 2022, **9**, 2203596.
10. S. Fang, A. Du, B. Zhou, Z. Liu, J. Nie, Y. Wang, H. Zhong, H. Hu, H. Li and Y. Shi, *Adv. Opt. Mater.*, 2023, **11**, 2202952.